Railway Engineering Science (2024) 32(2):244–256
https://doi.org/10.1007/s40534-023-00328-y

Low-frequency oscillation of train–network system considering traction power supply mode

Yuchen Liu[1] · Xiaoqin Lyu[1] · Mingyuan Chang[1] · Qiqi Yang[1]

Received: 19 July 2023 / Revised: 29 November 2023 / Accepted: 6 December 2023 / Published online: 19 February 2024

Abstract
The low-frequency oscillation (LFO) has occurred in the train–network system due to the introduction of the power electronics of the trains. The modeling and analyzing method in current researches based on electrified railway unilateral power supply system are not suitable for the LFO analysis in a bilateral power supply system, where the trains are supplied by two traction substations. In this work, based on the single-input and single-output impedance model of China CRH5 trains, the node admittance matrices of the train–network system both in unilateral and bilateral power supply modes are established, including three-phase power grid, traction transformers and traction network. Then the modal analysis is used to study the oscillation modes and propagation characteristics of the unilateral and bilateral power supply systems. Moreover, the influence of the equivalent inductance of the power grid, the length of the transmission line, and the length of the traction network are analyzed on the critical oscillation mode of the bilateral power supply system. Finally, the theoretical analysis results are verified by the time-domain simulation model in MATLAB/Simulink.

Keywords Low-frequency oscillation · Train–network system · Modal analysis · Bilateral power supply · Participation factor

1 Introduction

Electric trains connected to the traction network will introduce lots of power electronics, which may cause low-frequency oscillation (LFO) in the train–network system due to the interaction between the network and the power electronics of the trains [1, 2]. Therefore, the modeling of the traction power supply system is very important for the LFO stability analysis. Traction power supply system widely adopts the unilateral power supply mode, which exists a sectioning post between two adjacent traction substations. Trains will lose power over the sectioning post, which is one of the weakest links of the traction power supply system, therefore making it not suitable for the electrified railways with long ramps [3–5]. Taking electrified railways at high altitude as an example, the short circuit capacity of the power grid along the line is small, and each feeding section is long. When multiple trains are pulling uphill and braking downhill, it is easy to cause the catenary voltage drop and the voltage overrun, respectively, which cannot make a safe and stable operation of the running trains [6–8]. Studies have shown that the bilateral power supply mode with the cancelation of the sectioning post has the ability to realize long-distance power supply, and can improve the power supply capacity, especially for the electrified railways which are often connected to the weak power grid in the high-altitude areas [9–14]. However, the adoption of bilateral power supply mode which increases the length of the feeding sections will increase the number of connecting trains, and then increase the risk of system oscillation. The existing unilateral power supply technology of traction power supply system is not suitable for the construction of high-altitude mountain railway. Therefore, it is necessary to study the stability of trains connected to the bilateral power supply system and compare it with the trains connected to the unilateral power supply system.

In the existing studies, the train–network system adopting the unilateral power supply mode has been modeled as a single-phase voltage source, an equivalent impedance and the trains in Refs. [15–19]. Lv et al. [20], considering the complete structure of the traction network, established the

✉ Xiaoqin Lyu
xiaoqin93@163.com

[1] School of Electrical Engineering, Southwest Jiaotong University, Chengdu 610031, China

state space model of the train–network system and analyzed the stability by eigenvalue analysis method. In Ref. [21], based on the impedance-based method, which regarded the train–network system as a cascade system of the traction power supply system (source side) and the input impedance of the train (load side) [22], the *dq* impedance model of China CRH5 train considering the synchronous system, the current inner loop and the voltage outer loop has been established. Moreover, considering the second-order generalized integrator (SOGI) and phase-locked loop (PLL), a more accurate *dq* impedance model has been established, and the influence of different control links of CRH5 train on LFO has been analyzed in Ref. [23]. Chang et al. [24] built the single-input and single-output (SISO) impedance model of CRH5 train, which can express the relationship between the actual input voltage and current of the trains and has clear physical meaning. Then the SISO impedance has been used to establish the RLC circuit to analyze the influence of control parameters on impedance characteristics of the train. The existing studies based on the unilateral power supply mode have studied the mechanism of LFO and the influence of different parameters on oscillation, and many valuable conclusions have been obtained. However, the above models only have one source and are not suitable for the bilateral power supply system, in which the trains can take power from two adjacent traction substations at the same time. Moreover, most of LFO studies focuse on the situation that the trains raise pantograph at the same place, and only the on-board auxiliary equipment works, while stability under the situation of the trains running at different places also needs to be discussed. Especially for the bilateral power supply system, the increase in the number of running trains will increase the probability of LFO.

However, when trains are running, there is an impedance of the traction network between the two trains, so the topology of the network becomes complex. It should be noted that, the common impedance-based method is not suitable for the system with complex topology, due to the system cannot be easily equivalent to the source and load subsystems. To deal with it, the modal analysis method proposed in Ref. [25] has been used in power system stability analysis. The modal analysis method can analyze the stability of the system by establishing the system node admittance matrix, which can consider the actual network topology of the system and is suitable for the study of this paper. Qin and Xu [26] studied the multi-virtual synchronous machine grid-connected power–frequency oscillation by modal analysis. Moreover, modal analysis has also been applied to traction power supply system. In Ref. [27], based on modal analysis, the LFO of the traction power supply system connected to the three-phase power grid was analyzed, and the interaction between the two feeding sections and their interaction with the power grid was studied.

In order to analyze the LFO and its propagation characteristics of the train–network system under the actual network topology, the modal analysis method is applied in this paper to study the train–network system including the three-phase power grid, traction transformer, traction network and the trains, and different power supply modes are considered.

The contributions of this paper are as follows:

(1) Based on the train–network topologies of bilateral power supply and unilateral power supply modes, the system node admittance matrices in frequency-domain including three-phase power grid, single-phase traction transformer, traction network and multiple trains are established.
(2) The modal analysis method is adopted to study the LFO when multiple trains are running at different places, and the oscillation modes and propagation characteristics of the LFO under the bilateral and unilateral power supply modes are analyzed and compared.
(3) For the bilateral power supply system, the influences of the equivalent inductance of the power grid, the length of the transmission line and the length of the traction network on the LFO mode are studied.

The rest of this paper is arranged as follows. In Sect. 2, based on the SISO impedance model of CRH5 train, the equivalent circuits and the node admittance matrices of the bilateral and unilateral power supply systems are established. In Sect. 3, the oscillation modes and propagation characteristics of bilateral and unilateral power supply systems are analyzed and compared by modal analysis. The influences of different parameters on the oscillation mode are studied. In Sect. 4, the simulation results in MATLAB/Simulink are analyzed to prove the feasibility and correctness of the modal analysis. Finally, the conclusion is summarized in Sect. 5.

2 Model of train–network system considering the network topology

2.1 Main circuit structure and control strategy of the train

The train studied in this work is the CRH5 train, which has five power units with the same structures. The main circuit structure of two gird-side converters of each unit is shown in Fig. 1, where e_s and i_s are the primary voltage and current of on-board transformer, respectively; e and i are the secondary voltage and current of on-board transformer, respectively; R_n and L_n are the equivalent impedances of on-board transformer; C_d and R_d are the DC-side capacitor and load,

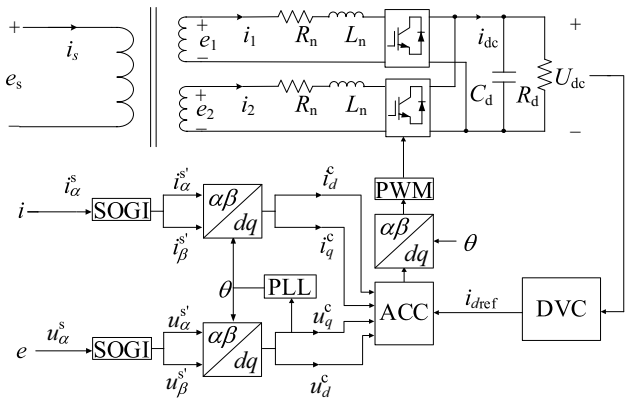

Fig. 1 The main circuit and control strategy of the grid-side converters

respectively; and U_{dc} and i_{dc} are the DC-side voltage and current respectively.

CRH5 train adopts *dq* decoupling control, which including second-order generalized integrator (SOGI), phase-locked loop (PLL), AC current controller (ACC), DC voltage controller (DVC) and pulse width modulation (PWM). θ is the phase of the converter input voltage; the subscript *dq* denotes the component in synchronous rotating frame; the subscript $\alpha\beta$ denotes the component in stationary frame; the superscript s represents the system component; the superscript s' represents the component obtained through the SOGI; the superscript c represents the control component in the control system; i_{dref} is the reference current of the ACC.

2.2 SISO impedance model of the train

SOGI converts input voltage and current components into $\alpha\beta$ components, as shown in Eq. (1):

$$\begin{cases} \Delta u_\alpha^s = \Delta e \\ \Delta u_\beta^s = \frac{\omega_0}{s}\Delta e \end{cases}, \quad \begin{cases} \Delta i_\alpha^s = \Delta i \\ \Delta i_\beta^s = \frac{\omega_0}{s}\Delta i \end{cases}. \tag{1}$$

where Δe, Δi, Δu_α^s, Δu_β^s, Δi_α^s and Δi_β^s are the small perturbations; and ω_0 is the fundamental frequency.

According to the Park transformation, the *dq* components of the small signal components of the input voltage and current small signal components can be obtained as

$$\begin{cases} \Delta u_d^s = \cos\omega_0 t \cdot \Delta u_\alpha^s + \sin\omega_0 t \cdot \Delta u_\beta^s \\ \Delta u_q^s = -\sin\omega_0 t \cdot \Delta u_\alpha^s + \cos\omega_0 t \cdot \Delta u_\beta^s \end{cases}, \\ \begin{cases} \Delta i_d^s = \cos\omega_0 t \cdot \Delta i_\alpha^s + \sin\omega_0 t \cdot \Delta i_\beta^s \\ \Delta i_q^s = -\sin\omega_0 t \cdot \Delta i_\alpha^s + \cos\omega_0 t \cdot \Delta i_\beta^s \end{cases}. \tag{2}$$

Reference [23] established the *dq* impedance model of the grid-side converter $\boldsymbol{Z}_{dq}(s)$, which can be written in second-order matrix form:

$$\begin{bmatrix} \Delta u_d^s \\ \Delta u_q^s \end{bmatrix} = \begin{bmatrix} Z_{dd}(s) & Z_{dq}(s) \\ Z_{qd}(s) & Z_{qq}(s) \end{bmatrix} \begin{bmatrix} \Delta i_d^s \\ \Delta i_q^s \end{bmatrix} \triangleq \boldsymbol{Z}_{dq}(s) \begin{bmatrix} \Delta i_d^s \\ \Delta i_q^s \end{bmatrix}, \tag{3}$$

where $\boldsymbol{Z}_{dq}(s)$ is an asymmetric matrix and has no practical physical meaning. In order to convert the impedance in the *dq*-frame to phase-domain, the second-order impedance matrix $\boldsymbol{Z}_{dq}(s)$ needs to be firstly transformed into two transfer functions $G_{dq+}(s)$ and $G_{dq-}(s)$ [28], which can be expressed as

$$\Delta u_d^s + \mathrm{j}\Delta u_q^s = \underbrace{\left(\frac{Z_{dd}(s)+Z_{qq}(s)}{2} + \mathrm{j}\frac{Z_{qd}(s)-Z_{dq}(s)}{2}\right)}_{G_{dq+}(s)} \left(\Delta i_d^s + \mathrm{j}\Delta i_q^s\right) \\ + \underbrace{\left(\frac{Z_{dd}(s)-Z_{qq}(s)}{2} + \mathrm{j}\frac{Z_{dq}(s)+Z_{qd}(s)}{2}\right)}_{G_{dq-}(s)} \left(\Delta i_d^s - \mathrm{j}\Delta i_q^s\right), \tag{4}$$

Due to $\Delta u_\beta = -\mathrm{j}\Delta u_\alpha$, $\Delta i_\beta = -\mathrm{j}\Delta i_\alpha$, the relationship between the input voltage and current components in $\alpha\beta$-frame is

$$\Delta u_\alpha^s + \mathrm{j}\Delta u_\beta^s = \underbrace{\mathrm{e}^{\mathrm{j}\omega_0 t} G_{dq+}(s) \mathrm{e}^{-\mathrm{j}\omega_0 t}}_{G_{\alpha\beta+}(s)} \left(\Delta i_\alpha^s + \mathrm{j}\Delta i_\beta^s\right) \\ + \underbrace{\mathrm{e}^{\mathrm{j}\omega_0 t} G_{dq-}(s) \mathrm{e}^{-\mathrm{j}\omega_0 t}}_{G_{\alpha\beta-}(s)} \left(\Delta i_\alpha^s - \mathrm{j}\Delta i_\beta^s\right). \tag{5}$$

According to Eq. (1), Δu_α^s, Δu_β^s, Δi_α^s and Δi_β^s can be represented by Δe and Δi. Thus, the relation between Δe and Δi can be obtained [24]:

$$\Delta e = \frac{(s+\mathrm{j}\omega_0)\cdot\left[Z_{aa}(s)+\mathrm{j}Z_{ab}(s)\right] + (s-\mathrm{j}\omega_0)\cdot\left[Z_{ba}(s)+\mathrm{j}Z_{bb}(s)\right]}{s+\mathrm{j}\omega_0} \\ \Delta i \triangleq Z_{\mathrm{unit}}\Delta i, \tag{6}$$

where Z_{unit} is the SISO impedance model of the grid-side converter, $Z_{aa}(s)$, $Z_{bb}(s)$, $Z_{ba}(s)$ and $Z_{bb}(s)$, respectively, are

$$\begin{cases} Z_{aa}(s) = \frac{Z_{dd}(s-\mathrm{j}\omega_0)+Z_{qq}(s-\mathrm{j}\omega_0)}{2}, & Z_{ab}(s) = \frac{Z_{qd}(s-\mathrm{j}\omega_0)-Z_{dq}(s-\mathrm{j}\omega_0)}{2} \\ Z_{ba}(s) = \frac{Z_{dd}(s-\mathrm{j}\omega_0)-Z_{qq}(s-\mathrm{j}\omega_0)}{2}, & Z_{bb}(s) = \frac{Z_{qd}(s-\mathrm{j}\omega_0)+Z_{dq}(s-\mathrm{j}\omega_0)}{2} \end{cases}. \tag{7}$$

Therefore, the impedance of the CRH5 train can be expressed as

$$Z_{\mathrm{CRH5}} = \frac{k_{\mathrm{CRH5}}^2}{10t} Z_{\mathrm{unit}}, \tag{8}$$

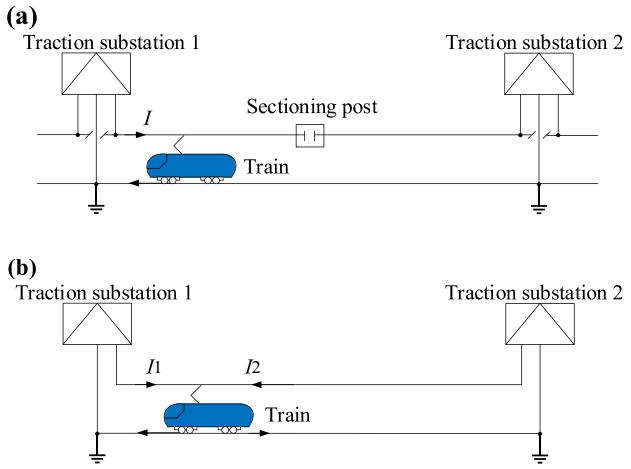

Fig. 2 Schematic diagrams of **a** the unilateral power supply system and **b** the bilateral power supply system

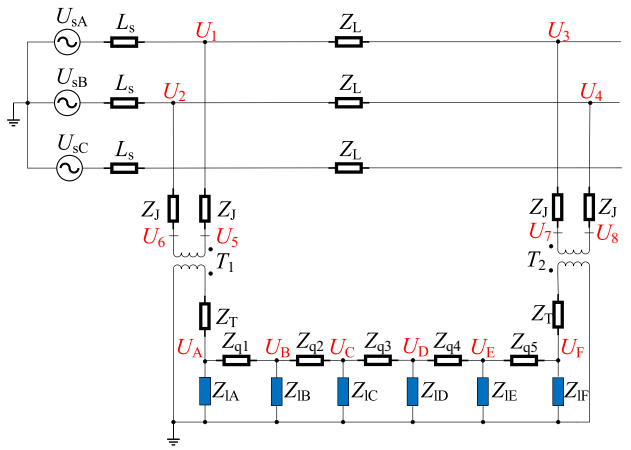

Fig. 3 Equivalent circuit of the bilateral power supply system

where $k_{CRH5} = 25{,}000/1770$ is the transformation ratio of the on-board transformer, and t is the number of the trains at the same position.

2.3 Models of unilateral and bilateral power supply system

There is a sectioning post between two adjacent traction substations in unilateral power supply system, so that the train can only take current from one traction substation. However, due to the cancelation of the sectioning post, the train can simultaneously take current from two adjacent traction substations in the bilateral power supply system, as shown in Fig. 2. Because the research object of this paper is only a feeding section of a traction substation, rather than two feeding sections of a traction substation. Therefore, a relatively simple single-phase transformer can be selected to supply power to this feeding section when establishing the model.

Figure 3 is the equivalent circuit of trains connected to the bilateral power supply system, which retains the actual network topology and considers the traction network impedance between two trains running at different places. Select nodes 1–8 as the nodes of three-phase grid side and U_1–U_8 denote the voltage of each node. Select nodes A–F as the nodes of traction network side and U_A–U_F denote the voltage of each node. U_{sA}, U_{sB} and U_{sC} are the voltages of the three-phase 220 kV power system; L_s is the power grid equivalent inductance; Z_L is the impedance of the 220 kV transmission line between two adjacent traction substations; Z_J is the power line equivalent impedance of the traction substations; T_1 and T_2 are single-phase traction transformers which represent traction substation 1 and traction substation 2, respectively; Z_T is the equivalent impedance of the single-phase traction transformer; Z_{q1}–Z_{q5} are the impedances of different segments of the traction network, and Z_{lA}–Z_{lF} are the impedances of the trains connected at nodes A–F, respectively.

In order to obtain the node admittance matrix of the bilateral power supply system, the nodes of the system are firstly divided into three types. Type I is nodes 1–4 of the high-voltage side of 220 kV transmission line, type II is nodes 5–8 of the high-voltage side of the single-phase traction transformers, and type III is nodes A–F of the low-voltage side of the traction network. The relationship between nodal voltages and currents is shown in Eq. (9):

$$\begin{bmatrix} I_{\mathrm{I}} \\ I_{\mathrm{II}} \\ I_{\mathrm{III}} \end{bmatrix} = \begin{bmatrix} Y_{\mathrm{I,I}} & Y_{\mathrm{I,II}} & Y_{\mathrm{I,III}} \\ Y_{\mathrm{II,I}} & Y_{\mathrm{II,II}} & Y_{\mathrm{II,III}} \\ Y_{\mathrm{III,I}} & Y_{\mathrm{III,II}} & Y_{\mathrm{III,III}} \end{bmatrix} \begin{bmatrix} U_{\mathrm{I}} \\ U_{\mathrm{II}} \\ U_{\mathrm{III}} \end{bmatrix} \triangleq \boldsymbol{Y} \begin{bmatrix} U_{\mathrm{I}} \\ U_{\mathrm{II}} \\ U_{\mathrm{III}} \end{bmatrix}, \tag{9}$$

where I_{I}, I_{II} and I_{III} are the nodal currents injection; U_{I}, U_{II} and U_{III} are the nodal voltages; $Y_{\mathrm{I,I}}$, $Y_{\mathrm{II,II}}$ and $Y_{\mathrm{III,III}}$ are the self-admittance matrices of these three types of nodes; $Y_{\mathrm{I,II}} = Y_{\mathrm{II,I}}$, $Y_{\mathrm{I,III}} = Y_{\mathrm{III,I}}$ and $Y_{\mathrm{II,III}} = Y_{\mathrm{III,II}}$ are the mutual admittance matrices of these three types of nodes; and $\boldsymbol{Y}$ is the system node admittance matrix.

In the unilateral power supply system, there is a sectioning post between two adjacent traction substations. For easy to compare, the names of nodes in the unilateral power supply system are consistent with those in the bilateral power supply system, as shown in Fig. 4. It should be noted that the

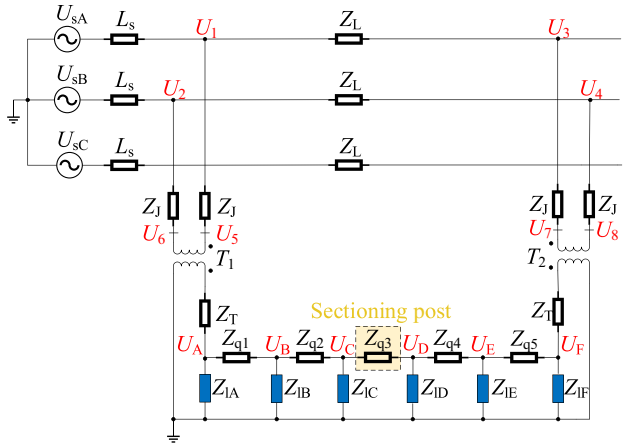

Fig. 4 Equivalent circuit of the unilateral power supply system

impedance of the traction network between node C and node D is regarded as infinite to simulate the state of two feeding sections disconnected. Similarly, the node admittance matrix of the unilateral power supply system can be obtained.

3 LFO study of the bilateral and unilateral power supply systems

3.1 Modal analysis

This paper analyzes the LFO of the bilateral and unilateral power supply systems by modal analysis [25]. Firstly, the SISO impedance model of the train and the equivalent circuit model of the train–network system should be established, and the system node admittance matrix $\boldsymbol{Y}$ can be obtained. In Eq. (9), the matrix $\boldsymbol{Y}$ can be decomposed into the following form [25]:

$$\boldsymbol{Y} = \boldsymbol{L}\boldsymbol{\Lambda}\boldsymbol{T}, \tag{10}$$

where $\boldsymbol{\Lambda}$ is the diagonal eigenvalue matrix, $\boldsymbol{L}$ and $\boldsymbol{T}$ are the left and right eigenvector matrices, respectively, and $\boldsymbol{L}=\boldsymbol{T}^{-1}$.

Defining $\boldsymbol{V}=\boldsymbol{T}\boldsymbol{U}$ as the modal voltage vector and $\boldsymbol{J}=\boldsymbol{T}\boldsymbol{I}$ as the modal current vector, respectively, and substituting Eqs. (10) into (9) yields

$$\begin{bmatrix} V_1 \\ V_2 \\ \vdots \\ V_n \end{bmatrix} = \begin{bmatrix} \lambda_1^{-1} & 0 & 0 & 0 \\ 0 & \lambda_2^{-1} & 0 & 0 \\ 0 & 0 & \vdots & 0 \\ 0 & 0 & 0 & \lambda_n^{-1} \end{bmatrix} \begin{bmatrix} J_1 \\ J_2 \\ \vdots \\ J_n \end{bmatrix}, \tag{11}$$

where the reciprocal of the eigenvalue λ_n^{-1} is defined as modal impedance, and the subscript number n represents the number of nodes.

According to Eq. (11), it can be seen that when λ_1^{-1} is much larger than other modal impedance, even a small current J_1 can produce a large voltage V_1. Therefore, the mode 1 is the critical oscillation mode. The left eigenvector L_{ni} and the right eigenvector T_{in} represent the observability and controllability of node n to mode i oscillation, respectively. The participation factor of node n to mode i oscillation is defined as $PF_{ni}=L_{ni}T_{in}$.

3.2 Comparison of oscillation modes between the bilateral and unilateral power supply systems

3.2.1 The bilateral power supply system with 6 trains connected

In the bilateral power supply system, 6 trains are connected to the traction network at different places, respectively, as shown in Fig. 3, which is called as bilateral power supply A1B1C1D1E1F1. Considering that trains on the same line depart at the same interval in actual railway operation, the impedances of the traction network between two trains are assumed to be the same value, that is $Z_{q1}=Z_{q2}=\ldots=Z_{q5}=Z_q$. The main parameters of the system are shown in Table 1. And the trains are operating at about 50% of the rated power. Based on modal analysis, the corresponding modal impedance frequency curve can be drawn, as shown in Fig. 5. The mode which has the largest modal impedance is the critical mode 1. It can be seen that the oscillation frequency of the critical mode 1 of the bilateral power supply A1B1C1D1E1F1 is 4.30 Hz, and the modal impedance of the critical mode 1 is 193.7 p.u.

3.2.2 The unilateral power supply system with 6 trains connected

In this case, the parameters of the system and the number of trains remain unchanged, and only a sectioning post is added between the two traction substations, which is the unilateral power supply system. This case is called as unilateral power supply A1B1C1D1E1F1. Similarly, the corresponding modal impedance frequency curve can be obtained, as shown in Fig. 6. It can be seen that the oscillation frequency of the critical mode 2 of the unilateral power supply A1B1C1D1E1F1 is 4.30 Hz, and the modal impedance is 208.6 p.u.

3.2.3 The unilateral and bilateral power supply systems with 3 trains connected, respectively

In order to further compare the difference of oscillation modes of the unilateral and bilateral power supply systems

Table 1 The main parameters of the system

Element	Symbol	Description	Value
The external circuit of gird-side converter	U_S	Phase-to-phase voltage of the power grid	220 kV
	L_S	Equivalent inductance of the power grid	0.24 H
	Z_L	Impedance of 220 kV transmission line	(0.4818 + j3.19)*5 Ω
	Z_J	Line impedance of high voltage side of the traction substation	(0.4818 + j3.19) Ω
	k	Transformation ratio of the traction transformer	220/27.5
	Z_T	Equivalent impedance of the traction transformer	(0.1581 + j1.985) Ω
	Z_q	Impedance of the traction network	(0.594 + j2.065) Ω
The main circuit of gird-side converter	R_n	Resistance of the train on-board transformer	0.165 Ω
	L_n	Inductance of the train on-board transformer	0.006 H
	C_d	DC link capacitance	0.009 F
	R_d	Load resistance	50 Ω
	U_{dc}	DC link voltage	3600 V
The controller of gird-side converter	K_{pu}/K_{iu}	PI control parameters of DVC	0.4/15
	K_{pi}/K_{ii}	PI control parameters of ACC	1.5/10
	K_{pPLL}/K_{iPLL}	PI control parameters of PLL	0.7/25
	K_{eSOGI}/K_{iSOGI}	P control parameters of SOGI	0.1/1

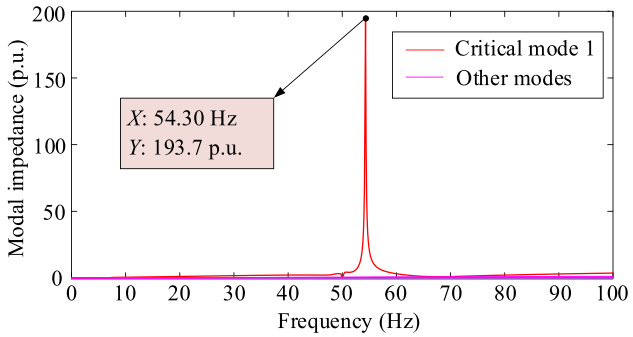

Fig. 5 The modal impedance frequency curve of bilateral power supply A1B1C1D1E1F1

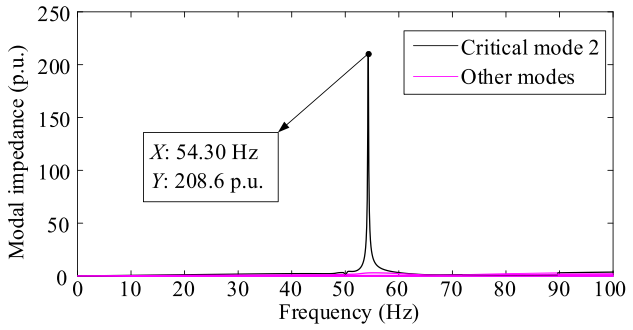

Fig. 6 The modal impedance frequency curve of unilateral power supply A1B1C1D1E1F1

and analyze the influence of the number of trains on oscillation mode, 3 trains are connected to nodes A, B and C of the traction network, respectively. The rest of parameters remain the same as the above. These two cases are called as unilateral power supply A1B1C1 and bilateral power supply A1B1C1, respectively.

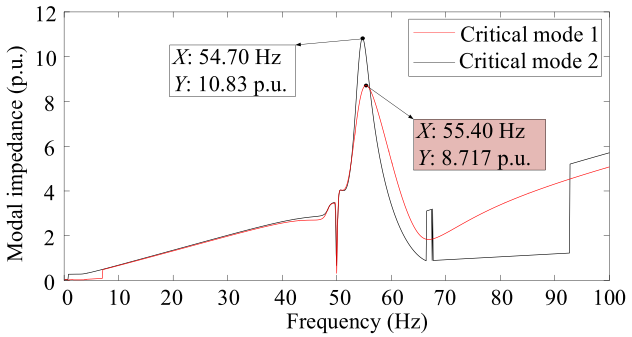

Fig. 7 The critical modal impedance frequency curve of unilateral power supply A1B1C1 and bilateral power supply A1B1C1

Figure 7 gives the comparison of the critical modal impedance frequency curves of unilateral power supply A1B1C1 and bilateral power supply A1B1C1. It can be seen that the oscillation frequency of the critical mode 2 of unilateral power supply A1B1C1 is 4.70 Hz, and the modal impedance is 10.83 p.u. The oscillation frequency of the critical mode 1 of bilateral power supply A1B1C1 is 5.40 Hz, and the modal impedance is 8.717 p.u.

The modal impedances and oscillation frequencies of the critical oscillation modes under different power supply modes and different numbers of running trains are summarized in Table 2. It can be concluded that when the power supply mode changes from bilateral to unilateral

Table 2 The critical oscillation modes of the train–network system under different power supply modes and different numbers of running trains

Case	The number of running trains	The largest modal impedance (p.u.)	Oscillation frequency (Hz)
Bilateral power supply A1B1C1D1E1F1	6	193.7	4.30
Unilateral power supply A1B1C1D1E1F1	6	208.6	4.30
Bilateral power supply A1B1C1	3	8.7	5.40
Unilateral power supply A1B1C1	3	10.8	4.70

Table 3 The participation factor, observability, controllability and harmonic content corresponding to the critical mode in the bilateral power supply system

Nodes		Theory			Simulation
		Participation factor	Observability	Controllability	Harmonic content (p.u.)
High-voltage side	1	0.0119	0.1089	0.1089	0.1424
	2	0.0119	0.1089	0.1089	0.1424
	3	0.0145	0.1202	0.1202	0.1567
	4	0.0145	0.1202	0.1202	0.1567
	5	0.0124	0.1112	0.1112	0.1456
	6	0.0124	0.1112	0.1112	0.1456
	7	0.0150	0.1224	0.1224	0.1596
	8	0.0150	0.1224	0.1224	0.1596
Low-voltage side	A	0.1001	0.3161	0.3161	0.4179
	B	0.1512	0.3885	0.3885	0.5091
	C	0.1839	0.4285	0.4285	0.5591
	D	0.1873	0.4324	0.4324	0.5622
	E	0.1601	0.3998	0.3998	0.5184
	F	0.1116	0.3338	0.3338	0.4321

power supply, the modal impedance of the critical mode will increase, which means the oscillation amplitude in the bilateral power supply system is smaller than that in the unilateral power supply system. When the number of running trains increases both in these two supply systems, the modal impedances of the critical modes will increase and the oscillation frequencies will decrease, which indicates that the increase in the number of running trains will increase the system oscillation amplitude and decrease the oscillation frequency.

3.3 The propagation characteristics of the LFO in unilateral and bilateral power supply systems

In order to analyze the propagation characteristics of oscillation both in traction network and power grid, based on unilateral power supply A1B1C1D1E1F1 and bilateral power supply A1B1C1D1E1F1, the participation factors, observability and controllability of each node for the critical oscillation mode are studied by modal analysis, and the results are summarized in Tables 3 and 4, respectively. It can be concluded that the participation factors, observability and controllability of the midpoint of the traction network in the bilateral power supply system (node D) and the position near the sectioning post in the unilateral power supply system (node D) are the largest. Therefore, the midpoint of the traction network of the bilateral power supply system and the position near the sectioning post of the unilateral power supply system can be regarded as the oscillation center. Whether it is bilateral or unilateral power supply, the participation factors, observability and controllability of the nodes on the low-voltage side are greater than the nodes on the high-voltage side of the traction transformer, and on the low-voltage side, the farther the nodes from the traction substation, the greater the participation factors, observability and controllability are. That is, the oscillation of nodes close to the oscillation center is more obvious, and the oscillation can propagate from the low-voltage side to the high-voltage side.

Table 4 The participation factor, observability, controllability and harmonic content corresponding to the critical mode in the unilateral power supply system

Nodes		Theory			Simulation
		Participation factor	Observability	Controllability	Harmonic content (p.u.)
High-voltage side	1	0.0118	0.1085	0.1085	0.1437
	2	0.0118	0.1085	0.1085	0.1437
	3	0.0146	0.1206	0.1206	0.1592
	4	0.0146	0.1206	0.1206	0.1592
	5	0.0123	0.1106	0.1106	0.1468
	6	0.0123	0.1106	0.1106	0.1468
	7	0.0152	0.1230	0.1230	0.1622
	8	0.0152	0.1230	0.1230	0.1622
Low-voltage side	A	0.0947	0.3074	0.3074	0.4135
	B	0.1391	0.3727	0.3727	0.4987
	C	0.1659	0.4069	0.4069	0.5437
	D	0.2053	0.4527	0.4527	0.5899
	E	0.1722	0.4146	0.4146	0.5402
	F	0.1171	0.3419	0.3419	0.4463

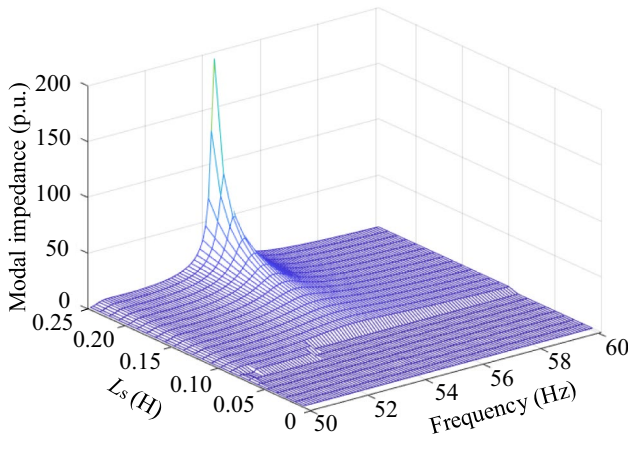

Fig. 8 Modal analysis results of the bilateral power supply system when L_s changes

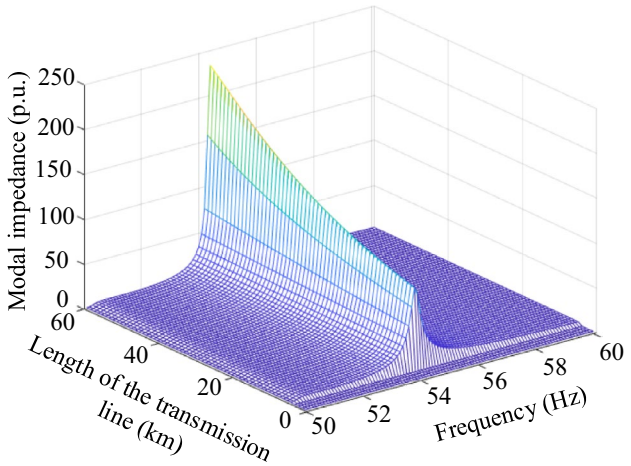

Fig. 9 Modal analysis results of the bilateral power supply system when the length of the transmission line changes

3.4 Influence of parameters on the critical mode of bilateral power supply system

3.4.1 Equivalent inductance of the power grid

In this case study, the influence of the power grid equivalent inductance (L_s) on the LFO is analyzed. Figure 8 shows the modal analysis results of the bilateral power supply system when L_s changes. It is shown in Fig. 8 that the modal impedance of the critical oscillation mode obviously increases and the oscillation frequency slightly decreases as L_s increases. The analysis result shows that with the increase of L_s, the oscillation amplitude will increase and the system will be more prone to oscillate.

3.4.2 Length of 220 kV transmission line

In this case study, the influence of the transmission line length on the LFO is analyzed. Figure 9 shows the modal analysis results of the bilateral power supply system when the length of the transmission line changes. It is shown in Fig. 9 that the modal impedance of the critical oscillation

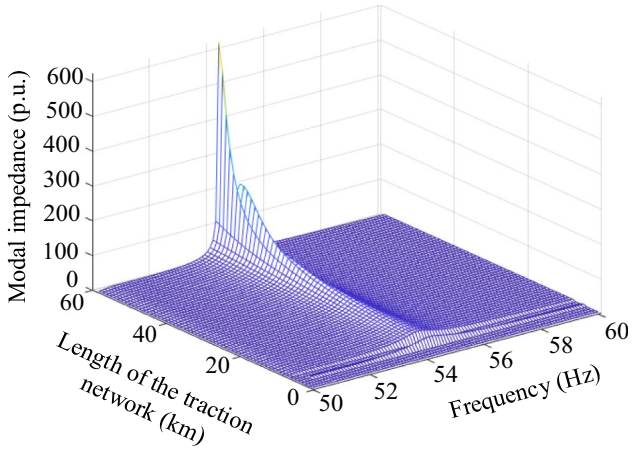

Fig. 10 Modal analysis results of the bilateral power supply system when the length of the traction network changes

mode slightly increases and the oscillation frequency remains unchanged as the length of the transmission line increases. The analysis result shows that with the increase in the length of the transmission line, the system is prone to oscillate; however, the influence is relatively smaller compared with the influence of the length of the traction network which will be discussed in next part.

3.4.3 Length of the traction network

In this case study, the influence of the lengths of the traction network on the LFO is analyzed. Figure 10 shows the modal analysis results of the bilateral power supply system when the length of the traction network changes. It is shown in Fig. 10 that the modal impedance of the critical oscillation mode obviously increases and the oscillation frequency slightly decreases as the length of the traction network increases. The analysis result shows that with the increase in the length of the traction network, the oscillation amplitude will increase and the system will be more prone to oscillate.

4 Simulation and verification

In order to verify the correctness of the above theoretical analysis, the time-domain simulation model of the train–network system was built in MATLAB/Simulink. By observing the waveforms of the DC-side voltage and network voltage of the converter, it is intuitive to judge whether the LFO occurs. This paper will verify the correctness of the modal analysis from two aspects. On the one hand, the simulation results are analyzed by ESPRIT method [29], which can obtain the oscillation frequency and the damping ratio of the system to verify the critical oscillation mode. On the other hand, the harmonic content of each node corresponding to the critical mode is obtained by FFT to verify the propagation characteristics of LFO.

Table 5 ESPRIT analysis results under different power supply modes

Power supply mode	Stability	Oscillation frequency (Hz)	Damping ratio
Bilateral power supply mode	Stable	4.89	0.1992
Unilateral power supply mode	Stable	4.84	0.1263

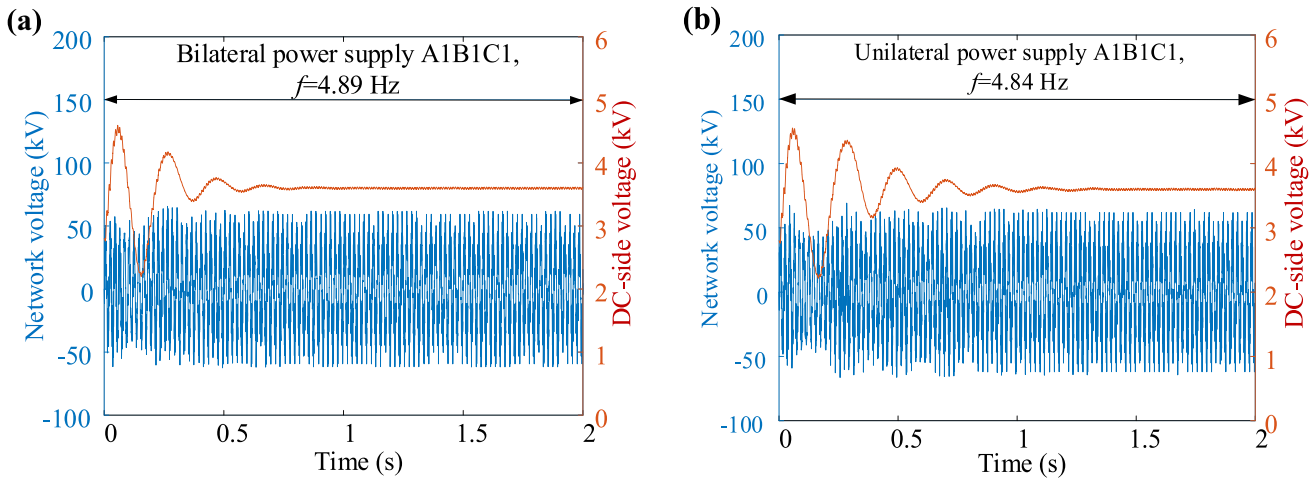

Fig. 11 The simulation results of the train at node A when the power supply mode changes: **a** bilateral power supply A1B1C1; **b** unilateral power supply A1B1C1

4.1 Influence of power supply mode

Figure 11 gives the simulation results of 3 trains are connected to node A, B and C, respectively, under the bilateral power supply mode and the unilateral power supply mode. It should be noted that, because the simulation results of the trains at different nodes are similar, this paper only shows the simulation results of the train at node A. Table 5 shows the ESPRIT analysis results under different power supply modes.

It is shown in Fig. 11 and Table 5 that, under the bilateral power supply mode, the waveform takes about 1 s to reach a stable state, while it takes about 1.5 s under the unilateral power supply mode. Moreover, the oscillation amplitude of the waveform under unilateral power supply mode is larger than that under bilateral power supply mode. This shows that when the number of running trains is the same, the bilateral power supply system is more stable than the unilateral power supply system. The simulation results are consistent with the theoretical analysis results in Table 2, which verifies the correctness of the theoretical analysis.

4.2 Influence of the number of running trains

Figure 12 shows the simulation results with 3 and 6 trains running, and Table 6 shows the ESPRIT analysis results under different numbers of running trains. It is shown in Fig. 12 and Table 6 that, when three running trains are connected to the system, the system is stable. While six running trains are connected to the system, the system has an oscillation with 4.12 Hz. The simulation results show that with the increase in the number of running trains, the oscillation frequency and damping ratio of the system will gradually decrease, and the stability of the system will be weakened. This is consistent with the theoretical analysis results in Table 2, which proves the correctness of the theoretical analysis.

Table 6 ESPRIT analysis results under different numbers of running trains

The number of running trains	Stability	Oscillation frequency (Hz)	Damping ratio
3	Stable	4.89	0.1992
6	Unstable	4.12	−0.0037

4.3 Simulation of propagation characteristics of LFO

In this subsection, FFT analysis is applied to obtain the harmonic content of each node at oscillation frequency when 6 trains connected to unilateral and bilateral power supply systems, respectively. The results are summarized in Tables 3 and 4. It can be seen that the harmonic content and observability of each node have the same change rules. The simulation results verify the conclusions of theoretical analysis, which proves the correctness of the model and analysis method.

4.4 Influence of the equivalent inductance of the power grid

The simulation results and the ESPRIT analysis results are shown in Fig. 13 and Table 7, respectively. It can be seen that the system will be stable due to its positive damping

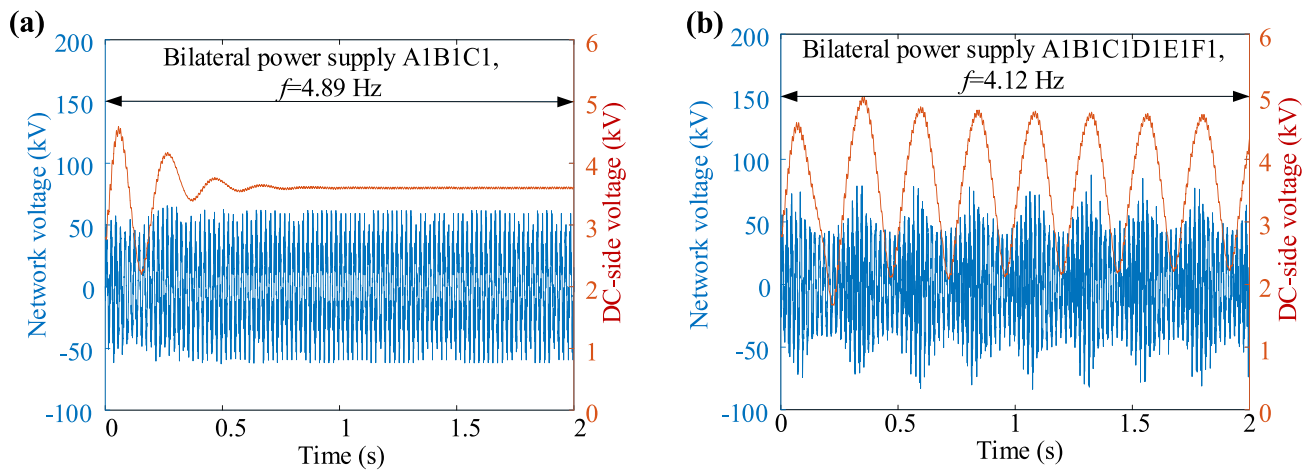

Fig. 12 The simulation results of the train at node A when the number of running trains changes: **a** bilateral power supply A1B1C1; **b** bilateral power supply A1B1C1D1E1F1

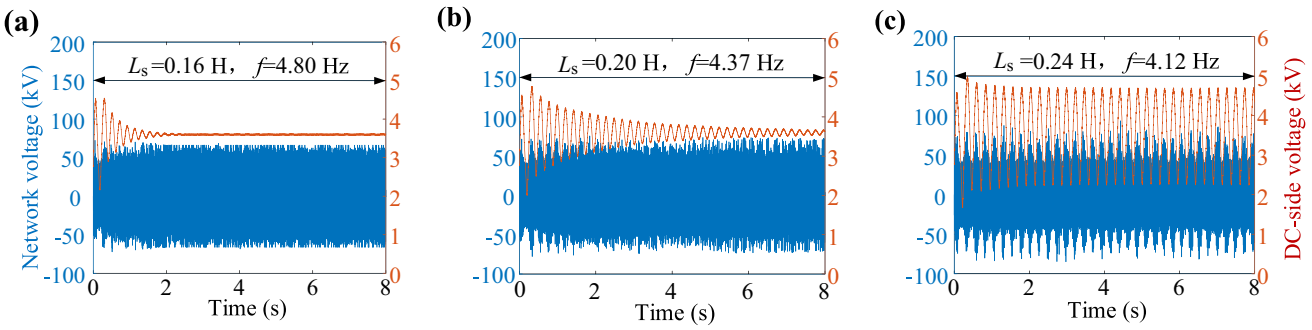

Fig. 13 The simulation results of the train at node A when L_s changes: **a** L_s = 0.16 H; **b** L_s = 0.20 H; **c** L_s = 0.24 H

Table 7 ESPRIT analysis results under different L_s

L_s (H)	Stability	Oscillation frequency (Hz)	Damping ratio
0.16	Stable	4.80	0.2675
0.20	Stable	4.37	0.1194
0.24	Unstable	4.12	−0.0037

Table 8 ESPRIT analysis results under different lengths of the transmission line

The length of the transmission line (km)	Stability	Oscillation frequency (Hz)	Damping ratio
40	Stable	4.14	0.0008
50	Unstable	4.12	−0.0037
60	Unstable	4.08	−0.0129

ratio when L_s is 0.16 H, while the system will have LFO due to its negative damping ratio when L_s is 0.24 H. Therefore, it can be considered that with the increase of L_s, the oscillation frequency and the damping ratio both decrease, which verifies the correctness of the theoretical findings.

4.5 Influence of the length of 220 kV transmission line

The simulation results and the ESPRIT analysis results are shown in Fig. 14 and Table 8, respectively. From Fig. 14 and Table 8, it can be seen that with the increase in the length of the transmission line, the oscillation frequency and the damping ratio both decrease slightly. Therefore, the waveforms obtained under different lengths of the transmission line are concatenated into one figure for easy comparison, which can also verify the correctness of the theoretical findings.

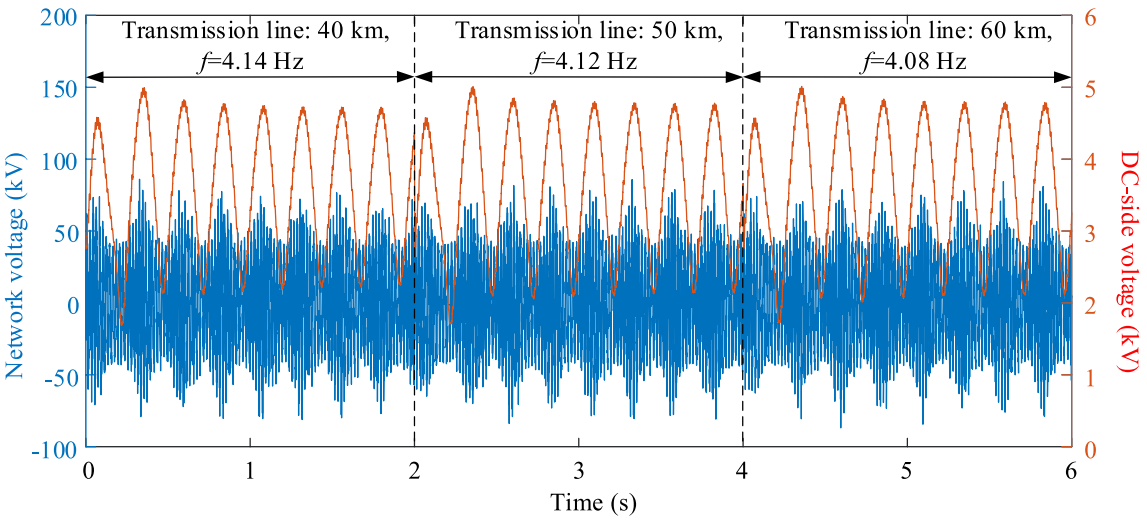

Fig. 14 The simulation results of the train at node A when the length of the transmission line changes

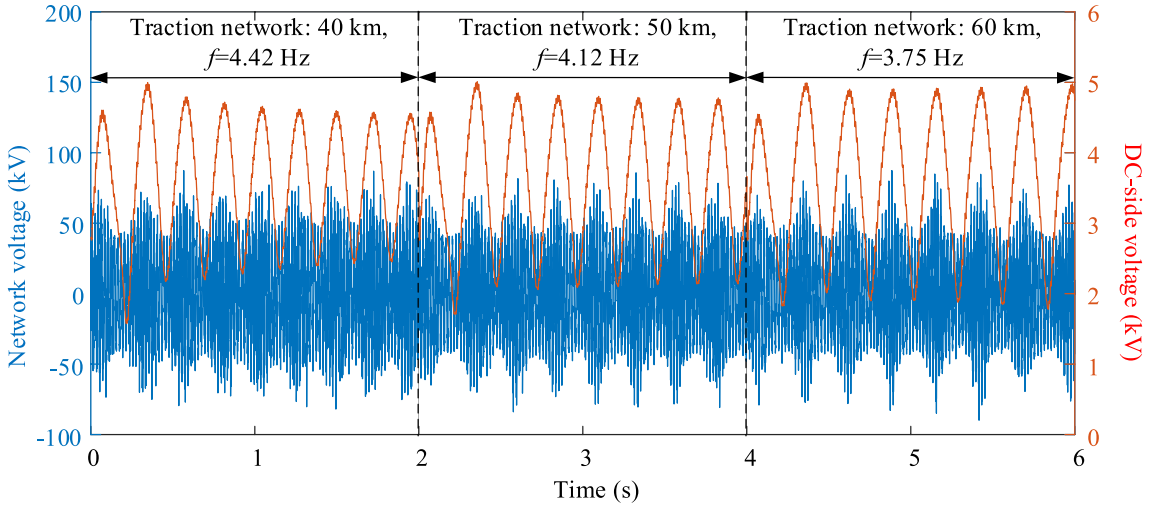

Fig. 15 The simulation results of the train at node A when the length of the traction network changes

Table 9 ESPRIT analysis results under different lengths of the traction network

Length of traction network (km)	Stability	Oscillation frequency (Hz)	Damping ratio
40	Stable	4.42	0.0782
50	Unstable	4.12	−0.0037
60	Unstable	3.75	−0.0257

4.6 Influence of the length of the traction network

The simulation results and the ESPRIT analysis results are shown in Fig. 15 and Table 9, respectively. From Fig. 15 and Table 9, it can be seen that with the increase in the length of the traction network, the oscillation frequency and the damping ratio both decrease. Therefore, the waveforms obtained under different lengths of the traction network are concatenated into one figure for easy comparison, which can also verify the correctness of the theoretical findings.

5 Conclusions

In this paper, considering the actual topology of the traction power supply system with the power grid, traction transformer, and the traction network, the node admittance matrices of the system with two different power supply modes are established. Then, the oscillation modes and propagation characteristics of bilateral and unilateral power supply system, and the influence of different factors on LFO in the bilateral power supply system are analyzed by modal analysis. The main conclusions can be drawn as follows:

(1) When the number of running trains is the same, the bilateral power supply system is more stable than the unilateral power supply system. The increase in the number of running trains will lead to the increase in the system oscillation amplitude, even cause system instability.

(2) No matter whether the bilateral or unilateral power supply mode is adopted, the oscillation intensity of the nodes on the traction transformer low-voltage side is stronger than that on the high-voltage side, and on the low-voltage side, the further away from the traction substation, the more obvious the oscillation of the nodes.

(3) For the bilateral power supply mode, the midpoint of the traction network is the oscillation center. For the unilateral power supply mode, the position near the sectioning post is the oscillation center. Therefore, installing the sensor at the midpoint of the traction network of the bilateral power supply system and the position near the sectioning post of the unilateral power supply system, respectively, will achieve great monitoring effect.

(4) The equivalent inductance of the power grid and the length of the traction network have obvious influence on the LFO of the bilateral traction power supply system, while the length of the transmission line between two traction substations has little influence on the system LFO.

This paper only considers the LFO of multiple trains running with the same traction power. The LFO of the same type of trains under different operating conditions or different types of trains running at the same time under bilateral power supply mode can be further analyzed.

Acknowledgements This work was supported by the Applied Basic Research Program of Science and Technology Plan Project of Sichuan Province of China (No. 2020YJ0252).

References

1. Wu S, Liu Z (2021) Low-frequency stability analysis of vehicle-network system with active power filter based on dq-frame impedance. IEEE Trans Power Electron 36(8):9027–9040
2. Hu H, Tao H, Blaabjerg F et al (2018) Train–network interactions and stability evaluation in high-speed railways—part I: phenomena and modeling. IEEE Trans Power Electron 33(6):4627–4642
3. Liu Z, Meng X, Zhang Q et al (2023) Issues, challenges and countermeasures in traction power supply system of high-altitude mountain railway. Power Syst Technol 47(05):2039–2054 (in Chinese)
4. Lu C, Cai C (2019) Challenges and countermeasures for construction safety during the Sichuan–Tibet railway project. Engineering 5(5):833–838
5. Zhang Q, Zhang Y, Ke H et al (2022) Modeling of regenerative braking energy for electric multiple units passing long downhill section. IEEE Trans Transp Electrif 8(3):3742–3758
6. Deng Y, Lin Z (2019) Thoughts on challenges faced by Sichuan–Tibet railway electrification project and its solutions. Electr Railw 30(S1):5–11 (in Chinese)
7. Yan H, Xie S, Wang H et al (2022) Research on tree bilateral continuous power supply scheme and its application. Electr Power Autom Equip 42(5):191–197
8. Zhou Z (2020) Cophase connected power supply scheme of heavy haul railway based on tree bilateral power supply. J Railw Sci Eng 17(3):722–731
9. Meng X, Xia W, Deng Y, Liu Z (2021) Low-frequency oscillation research of Sichuan–Tibet railway under bilateral power supply for mixed passenger and freight locomotives operation. In: Proceedings of the 5th International Conference on Electrical Engineering and Information Technologies for Rail Transportation (EITRT), Qingdao, Oct. 22 - 24, 2021. Springer pp 607–616
10. Li Q, Wang H, Xie S (2021) Discussion on application of bilateral power supply technology on electrified railway. Electr Railw 32(6):1–4 (in Chinese)
11. Zhang L, Li X, Liang S et al (2022) Research on the influence of electric railway bilateral power supply on power system and countermeasures. Int J Electr Power Energy Syst 137:107769
12. Wang F, Wu M, Zhang S (2020) Research on bilateral power supply technology of electrified railway. In: Asia Energy and Electrical Engineering Symposium (AEEES), Chengdu, pp 311–317
13. Fan H (2015) Performance analysis of double-sided power supply system for electrified railway. Dissertation, Southwest Jiaotong University (in Chinese)
14. Li X, Liu J, Chen C et al (2022) Research on analysis of voltage loss of parallel bilateral power supply system and countermeasures. Proc CSU-EPSA 34(11):92–99
15. Zhou Y, Hu H, Yang X et al (2019) Low-frequency oscillation traceability and suppression in railway electrification systems. IEEE Trans Ind Appl 55(6):7699–7711
16. Hu H, Tao H, Wang X et al (2018) Train–network interactions and stability evaluation in high-speed railways—part II: Influential factors and verifications. IEEE Trans Power Electron 33(6):4643–4659
17. Kong R, Lyu X, Wang X et al (2023) Modeling and analysis of low-frequency oscillation in train–network system under mixed operation of trains. Proc CSEE 43(10):3768–3780 (in Chinese)
18. Frutos P, Ladoux P, Roux N et al (2022) Low frequency stability of AC railway traction power systems: analysis of the influence of traction unit parameters. Electronics 11(10):1593
19. Meng Z, Hu H, Zhou Y (2022) Study on the influence of electric locomotive operating conditions on low frequency oscillation of vehicle network System. J Electr Eng 17(2):131–141 (in Chinese)
20. Lv X, Wang X, Che Y et al (2019) Eigenvalue-Based harmonic instability analysis of electrical railway vehicle–network system. IEEE Trans Transp Electrif 5(3):727–744
21. Wang H, Wu M, Sun J (2015) Analysis of low-frequency oscillation in electric railways based on small-signal modeling of vehicle–grid system in *dq* frame. IEEE Trans Power Electron 30(9):5318–5330
22. Wang X, Blaabjerg F (2019) Harmonic stability in power electronic based power systems: concept, modeling, and analysis. IEEE Trans Smart Grid 10(3):2858–2870
23. Liao Y, Liu Z, Zhang H et al (2018) Low-Frequency stability analysis of single-phase system with dq-frame impedance approach—part I: impedance modeling and verification. IEEE Trans Ind Appl 54(5):4999–5011
24. Chang M, Wang X, Lv X, et al (2022) SISO impedance modeling of vehicle-grid system for low-frequency oscillation analysis. In: 2022 IEEE Power & Energy Society General Meeting (PESGM), Denver, pp 1–5
25. Wilsun Xu, HuangCui ZYu et al (2005) Harmonic resonance mode analysis. IEEE Trans Power Deliv 20(2):1182–1190
26. Qin B, Xu Y (2021) Modal Analysis of multi-virtual synchronous machine grid-connected power-frequency oscillation. Proc CSEE 41(19):6570–6580 (in Chinese)
27. Chang M, Wang X, Lv X et al (2023) Modeling and low-frequency oscillation analysis of an asymmetrical traction power system connected to power grid. IEEE Trans Transp Electrif 9(1):1750–1746
28. Wang X, Harnefors L, Blaabjerg F (2018) Unified impedance model of grid-connected voltage-source converters. IEEE Trans Power Electron 33(2):1775–1787
29. Roy R, Kailath T (1989) ESPRIT-Estimation of signal parameters via rotational invariance techniques. IEEE Trans Acoust Speech Signal Process 37(7):984–995